Radiation Protection Dosimetry (2018), pp. 1–13 doi:10.1093/rpd/ncx296

DEVELOPMENT OF A SET OF MESH-BASED AND AGE-DEPENDENT CHINESE PHANTOMS AND APPLICATION FOR CT DOSE CALCULATIONS

Yifei Pi[1], Tianyu Liu[2] and X. George Xu[1,2,*]
[1]School of Nuclear Science and Technology, University of Science and Technology of China, Hefei, Anhui Province 230026, PR China
[2]Nuclear Engineering Program, Rensselaer Polytechnic Institute, Troy, NY 12180, USA

*Corresponding author: xgxu@ustc.edu.cn

Received 7 October 2017; revised 3 December 2017; editorial decision 4 December 2017; accepted 14 December 2017

Phantoms for organ dose calculations are essential in radiation protection dosimetry. This article describes the development of a set of mesh-based and age-dependent phantoms for Chinese populations using reference data recommended by the Chinese government and by the International Atomic Energy Agency (IAEA). Existing mesh-based RPI adult male (RPI-AM) and RPI adult female (RPI-AF) phantoms were deformed to form new phantoms according to anatomical data for the height and weight of Chinese individuals of 5 years old male, 5 years old female, 10 years old male, 10 years old female,15 years old male, 15 years old female, adult male and adult female—named USTC-5 M, USTC-5F, USTC-10M, USTC-10F, USTC-15M, USTC-15F, USTC-AM and USTC-AF, respectively. Following procedures to ensure the accuracy, more than 120 organs/tissues in each model were adjusted to match the Chinese reference parameters and the mass errors were within 0.5%. To demonstrate the usefulness, these new set of phantoms were combined with a fully validated model of the GE LightSpeed Pro 16 multi-detector computed tomography (MDCT) scanner and the GPU-based ARCHER Monte Carlo code to compute organ doses from CT examinations. Organ doses for adult models were then compared with the data of RPI-AM and RPI-AF under the same conditions. The absorbed doses and the effective doses of RPI phantoms are found to be lower than these of the USTC adult phantoms whose body sizes are smaller. Comparisons for the doses among different ages and genders were also made. It was found that teenagers receive more radiation doses than adults do. Such Chinese-specific phantoms are clearly better suited in organ dose studies for the Chinese individuals than phantoms designed for western populations. As already demonstrated, data derived from age-specific Chinese phantoms can help CT operators and designers to optimize image quality and doses.

INTRODUCTION

Methods for estimating patient organ doses from computed tomography (CT) are one important topic of radiation protection, owing to the rapid increase of scans performed in the USA, Europe and China in the past decade. Surveys suggest that CT has become a major source of medical radiation exposure[(1–3)], responsible for more than 50% doses of the medical exams in the United States[(4–6)]. The core of this research was the estimation of organ dose information from such clinically important procedures. Radiation dosimetry is the basic science determining the amount and distribution of ionizing energy deposited in the interested objects. Accurate radiation dosimetry in the human body is quite challenging as discussed in a review article and a book by Xu *et al.*[(7, 8)]. Since organ doses cannot be directly measured in a live person, physical anthropomorphic phantoms have been used as a substitute for the sake of inserting dosimeters for pointwise dose measurement. It is well known that experimental and radiation safety procedures make in-phantom measurement expensive and time-consuming. For this reason, computational phantoms—a mathematical model of the human body—are more frequently used in organ dosimetry. As Xu observed[(7)], since the 1960s, three generations of computational phantoms have been reported: (1) stylized phantoms that are based on quadratic equations (1960–2000s); (2) voxel phantoms that are based on tomographic images (1980s–present); and (3) boundary representation (BREP) phantoms that are based on the advanced primitives which are easy to deform the geometrical shapes (2000s–present). The first-generation computational phantoms, known as the MIRD stylized models[(9)], were originally developed for estimating doses from internally deposited radioactive materials in workers and patients[(10)]. Although stylized phantoms made it possible to carry out Monte Carlo (MC) computations when computers were much less powerful, the original developers recognized the obvious shortcomings. It is too complex to realistically model the human anatomy with a limited set of surface equations[(7, 11)]. In the early 1980s, powerful computer and tomographic imaging technologies such as CT and magnetic resonance imaging (MRI) allowed researchers to visualize the internal structures of the body in 3D and to store the images in versatile digital formats. These led to the second-generation voxel phantoms that were realistic in depicting the anatomy of a specific individual. It is extremely inefficient to adjust the anatomical information in the voxel format, so the BREP phantoms—in the form of either non-uniform rational B-spline (NURBS) or polygonal meshes—become the latest research tool for organ dose calculations[7, 8, 12]. For the purposes of radiation protection, the 'Reference Man' methodology issued by the International Commission on Radiological Protection (ICRP) requires a computational phantom to match with the 50th percentile values in terms of body height and weight for a specific population group, including a specific gender or even a specific age group[13]. The RPI adult male (RPI-AM) and RPI adult female (RPI-AF)[14] phantoms we previously developed were based on the mesh geometry and carefully adjusted to match the parameters[13] defined for the ICRP 'Reference Man'[15]. Other studies used similar methods to create hundreds of BREP phantoms as are summarized in a review paper[7]. Particularly, children are generally considered to suffer more risks than adults under the same radiation conditions due to their higher radiation sensitivity in some growing organs and the increased likelihood for radiation-induced tumors, such as leukemia, brain, breast, skin and thyroid cancers[16] in their longer rest of life[17–20]. Owing to the attractive features in flexibility of the BREP phantoms, more phantoms with different ages and genders have emerged through manual and semiautomatic adjustments of mesh surfaces based on the existing reference phantoms[21–25]. For phantoms with different ages, Christ *et al.* constructed 'Virtual Family' phantoms (an adult male, an adult female and two children) based on high-resolution magnetic resonance images[26]. Lee *et al.*[27] used NURBS and polygon mesh to model six new pediatric hybrid phantoms: 1, 5 and 10-year-old males and females and Gayer *et al.*[28] has applied them to CT dosimetry. However, most of the existing BREP computational phantoms are based on the western populations parameters recommended by the ICRP, which differ from the Asian population[29–32]. There are several voxel Chinese phantoms such as CNMAN, VCH, CVP, CAM and CPP01[33–38]. Currently, no BREP phantoms for Chinese minors were reported.

Furthermore, computational phantoms must be coupled with a MC code that simulates radiation transport inside the human body for radiation dosimetry. The MC method is known to be credibly accurate in radiological physics[7]. Some public-domain, general-purpose MC codes have been employed including EGSnrc[39], FLUKA[40], GEANT4[41], MCNPX[42] and PENELOPE[43]. compared with the other types of radiation transport calculations. The drawback, however, is the lengthy time it takes to yield acceptable statistical precision[44, 45] through the extremely large number of particles in the simulation. In a revolutionary approach, we have demonstrated a new parallel MC method, ARCHER, which can be used in CPU, GPU or MIC platform to accelerate MC calculations[46–48].

In the area of commercially available software for CT organ doses reporting, ImPACT[49], CT-Expo[50], SimDoseCT[51] and VirtualDose[52, 53] are the most widely used tools. VirtualDose, used by more than 1000 users worldwide, was based on a family of 25 voxel phantoms and BREP phantoms that contain detailed anatomical information. The advanced 'software as a service (SaaS)' mode was chosen to design the interface to achieve the quick and easy accesses and maintenances[53]. Therefore, VirtualDose represents the state-of-the-art CT organ dose-reporting tool today.

This paper reports a major project undertaken in China to develop one of the first sets of mesh-based and age-dependent phantoms representing the Chinese population. Besides, the applications of these phantoms for CT dose calculations were described and the age-dependent organ doses were compared with the earlier published data by our group about the VirtualDose software. It is our hope that these phantoms and the derived organ dose information can help to meet the needs in China where nuclear power industry and medical imaging are growing rapidly.

MATERIALS AND METHODS

This section provides details in two parts: phantom development and application for CT dose calculations.

Phantom development

The phantom development includes the following steps (as illustrated in Figure 1):

(1) Evaluation of the initial input data including human body dimensions for Chinese adults and minors, reference organ volumes, tissue components and the original RPI-AM/RPI-AF phantoms.
(2) Adjustment of human body dimensions though scaling.
(3) Quality assurance (QA) to guarantee the accuracy in the newly created phantom.
(4) Preparation for dose calculations through voxelization of mesh-based the new phantom and assignment of tissue components.

Evaluation of initial input data

This study takes advantage of the RPI-AM and RPI-AF, previously developed at Rensselaer Polytechnic Institute[14]. Each phantom contains up to 140 organs or tissues, and is adjusted to match the ICRP reference values[13]. Since these phantoms were designed entirely with polygonal mesh surfaces, it is easy to change the size and the shape of organs. The original developers have already demonstrated the flexibility in morphing these original phantoms into overweight and obese phantoms, as well as female phantoms with different breast sizes(21–23). Therefore, it is a natural choice to use the original RPI-AM and RPI-AF phantoms in this study to create a set of Chinese phantoms by considering anatomical parameters that are specific to the Chinese population.

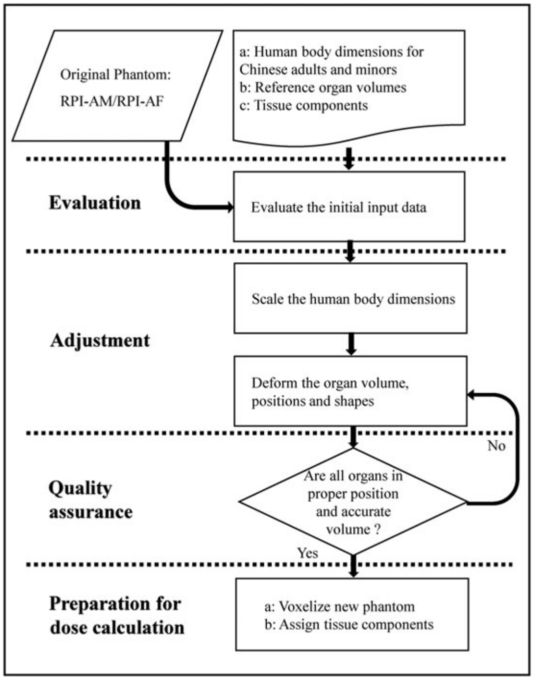

Figure 1. Steps in the development of mesh-based and age-dependent Chinese phantoms.

Such Chinese-specific data in our study are originated from the related Chinese standards and the International Atomic Energy Agency (IAEA) reports. Considering the ICRP reports regarding human anatomical parameters for the sake of radiation protection(13, 15, 54), the Chinese government issued reference data for its own population in 2007, which became the national standards later(29, 55, 56). A portion of the organ mass data from these Chinese standards are re-produced in Tables 1 and 2. However, walled-organ contents and some radiation insensitive tissues, such as muscles and vessel are not defined in the Chinese standards. To complement the data in Chinese standards, data from IAEA published in 1998 were further accepted in this study(30, 31). The IAEA data, include a set of anatomical, physiological and metabolic data for 'Reference Asian Man' covering the following age groups: newborn, 1-year old, 5-year old, 10-year old and adult from 20- to 50-year old in a similar definition as in the ICRP publications(13, 15, 57). A group of Chinese researchers from Tsinghua University adopted the IAEA organ or tissue data in a Chinese adult male phantom(36), as supplements of the Chinese standards. Table 3 summarizes the IAEA data adopted in this study. The skeleton is a heterogeneous mixture consisting of three parts, cortical bones, spongiosa bones and medullary cavities. Zankl *et al.*(58) demonstrated the effectiveness of the simplified method in modeling the skeleton when they constructed 'Rex' and 'Regina' phantoms. Because the existing Chinese standards and reference Asian data

Table 1. Reference mass values (g) of radiosensitive organs/tissues recommended by the Chinese government(55).

Organ/tissue	5-year		10-year		15-year		Adult	
	M	F	M	F	M	F	M	F
Testicles[a]	3.1	—	4.7	—	33	—	40	—
Ovaries[a]	—	0.5	—	1.4	—	9.8	—	11
RBM[b]	305	305	710	710	900	750	1100	800
Colon	102	102	170	170	291	225	310	240
Lungs[a]	360	360	580	580	940	720	1250	960
Stomach	47	47	75	75	120	95	145	110
Urinary bladder	13	13	21	21	38	30	40	30
Mammary gland	—	—	38	38	—	200	—	300
Liver	575	575	850	850	1170	1050	1410	1290
Esophagus	13	13	25	25	30	28	40	30
Thyroids	3.4	3.4	7.9	7.9	12	12	20	17
Skin	775	775	1200	1200	2200	1700	2400	1800
Bone surface	—	—	—	—	—	—	100	90

[a]Bilateral organs/tissues.
[b]RBM = red bone marrow.

Table 2. Reference mass values (g) of other organs/tissues for Chinese[55].

Organ/tissue	5-year		10-year		15-year		Adult	
	M	F	M	F	M	F	M	F
Body fat	1900	1900	5000	5000	6500	9000	9000	12 500
LBW[b]	17 100	17 100	27 000	27 000	48 500	41 000	54 000	41 500
Skeleton	2200	2200	4500	4500	7300	5700	8000	6000
Brain	1200	1200	1350	1350	1480	1360	1460	1330
Heart	95	95	150	150	240	200	325	290
Kidneys[a]	115	115	175	175	230	220	290	260
Spleen	70	70	100	100	140	120	165	150
Sialaden[a]	26	26	45	45	77	59	82	62
Gall bladder	3	3	4	4	8	6	9	7
Small intestine	190	190	325	325	540	420	620	450
Pancreas	40	40	60	60	90	75	120	100
Eyes[a]	13	13	14	14	15	12	15	12
Eye lens[a]	0.35	0.35	0.35	0.35	0.4	0.35	0.4	0.35
Adrenal gland[a]	5	5	6	6	10	10	14	13
Thymus	33	33	37	37	37	32	30	27
Pituitary gland	0.3	0.3	0.4	0.4	0.53	0.61	0.7	0.8
Body weight	19 000	19 000	32 000	32 000	55 000	50 000	63 000	54 000
Body fat	1900	1900	5000	5000	6500	9000	9000	12 500
LBW[a]	17 100	17 100	27 000	27 000	48 500	41 000	54 000	41 500
Skeleton	2200	2200	4500	4500	7300	5700	8000	6000

[a]Bilateral organs/tissues.
[b]LBW = lean body mass.

Table 3. Reference mass values (g) of organs/tissues for Asian Reference Man[30, 31].

Organ/tissue	5-year		10-year		15-year		Adult	
	M	F	M	F	M	F	M	F
Colon contents	120	120	190	190	340	260	360	280
Stomach contents	80	80	130	130	230	170	240	180
Bladder contents	33	32	54	54	96	78	100	85
Heart contents	130	130	210	220	380	290	400	300
Gall bladder contents	16	16	27	29	47	36	50	38
Small intestine contents	190	190	190	190	330	260	350	270
Rectum	6	6	10	10	19	19	20	20
Prostate	1	—	1.5	11	—	12	—	
Prostate contents	0.34	—	0.51	—	3.6	—	4	—
Tongue	64	50	67	51	67	51	67	51
Tonsil	1	0.98	1	1	4	3	4	3
Bronchus	8.5	8.3	14	15	24	18	26	20
Trachea	3.2	2.9	5	5	8	6	9	6.8
Ureter	5.1	4.9	8	8.6	13	14	14	15
Uterus	—	5.9	—	8.9	—	63	—	70
Spinal cord	20	20	30	30	30	30	30	30
Teeth	45	34	45	34	45	34	43	34

do not contain the certain information, the ICRP proportion data of bones were employed to calculate the mass of red bone marrow (RBM), yellow bone marrow (YBM), trabecular and cortical bones of every piece of the skeleton.

Adjustment of human body dimensions

The original RPI-AM and RPI-AF phantoms, which represent adults, were scaled to yield new phantoms with desired heights as illustrated in Figure 2. As shown in this figure, a phantom is divided into four

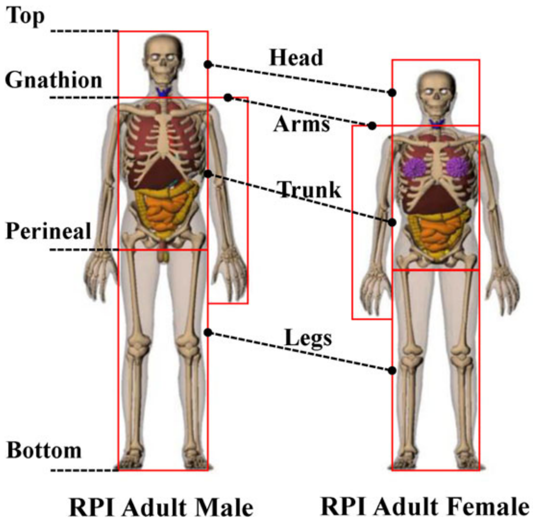

Figure 2. Different scaling factors for four phantom sections are specified.

sections: the head, the arms, the trunk and the legs. The ICRP has suggested that these four sections of the human body grow with different rates at different ages[13]. The growth rate is much slower after age 18 for boys and age 16 for girls[13, 59]. It is reasonable, therefore, to deform phantoms among adults with a uniform scaling factor suitable for these four sections. For adolescents, growth and development occur more rapidly for arms, legs and trunk. Figure 2 displays these sections of the phantom where different scaling factors are specified. According to the length, width and height of each section, the following scaling factors were calculated:

$$\begin{aligned} \text{WFactor} &= (\text{TargetWidth})/(\text{OriginalWidth}) \\ \text{HFactor} &= (\text{TargetHeight})/(\text{OriginalHeight}) \\ \text{LFactor} &= (\text{TargetLength})/(\text{OriginalLength}) \end{aligned} \tag{1}$$

where TargetWidth is the reference width of one model part, OriginalWidth represents the actual width value. TargetHeight, OriginalHeight, TargerLength and OriginalLength have similar significances. The new vertexes simply can be calculated by dot products with calculated factors.

After that, all the phantom sections were assembled to form a whole phantom. In-house MATLAB scripts were developed to automate these steps. Some reparative attempts were finally taken to fix gaps and to smooth the discrete commissures.

Quality assurance

The phantom adjustment steps were repeated to fix geometric errors caused by mismatches between the target phantom and the reference data. A QA measurement was undertaken to make sure the internal organ volumes indeed agreed with the desired reference parameters, and the 3D rendering of the phantom was performed with the help of the Rhinoceros software[60] to visually inspect the anatomical details. Organ volume calculations were finished by decomposing it into several elementary tetrahedrons[21] and were compared with reference organ parameters as summarized in Tables 1–3. The positions of inner organs and tissues were carefully checked according to human atlas of the Chinese people in this study[32]. Specific fine-tuning techniques, such as mesh offset, mesh scale and box edit operations were used to change an organ's volume and shape until organ-level parameters agreed within 0.5% with the reference Chinese data. Figure 3 demonstrates the deformation techniques in Rhinoceros software. Organ overlap was a frequent challenge and had to be carefully examined throughout the process. Subtraction of the Boolean operations was applied to circumvent the situation, when an overlap was identified.

Preparation for dose calculations

The tissue element compositions were defined for the purposes of radiation transport simulations involving MC methods. Organ-specific element compositions were based on reference values of the Chinese standard and the ICRU report 46[56, 61]. A C++/C# based voxelization tool[14] was used to convert the meshed-based age-dependent phantoms into voxel formatted phantoms. A voxel of 0.2 cm (8×10^{-3} cm^3) is selected to balance the geometrical accuracy and computational time for every new phantom. The organ volumes were found to be in good agreement <1% with the reference parameters after voxelization.

CT dose calculations

Archer MC dose calculation software

For this project, the ARCHER code was used for accurate and fast MC simulation[62]. The code has multi-GPU support, written in a hybrid of Open Multi-Processing (OpenMP) and CUDA. Each OpenMP thread on the CPU manages one GPU. Particle transport is run in parallel by many CUDA threads on each GPU. A Python script was written to perform thousands of instances of simulations in sequence that used different sets of parameters. For CT dose calculations in this study, only the photon

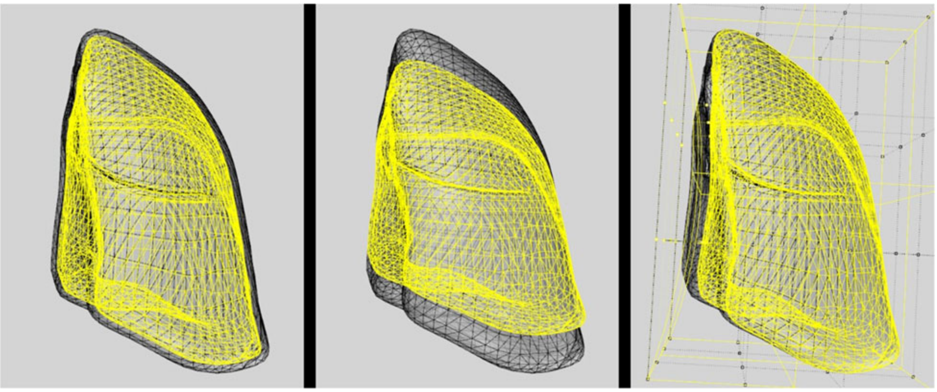

Figure 3. Mesh offset (left), mesh scale (middle) and box edit (right) operations in Rhinoceros. The original models were colored with black while it is yellow for the deformed models.

transport was enabled. Photoelectric effect, Compton scattering and Rayleigh scattering were explicitly simulated. In order to improve the accuracy of scattering simulation, the electron's binding effect was taken into account. Specifically, the angular distribution of scatter photons was modified by form factors, which tends to reduce the scattering cross-section in the forward direction for Compton scattering, and in the backward direction for Rayleigh scattering(42). The energy of secondary electrons was assumed to be deposited in the local voxels. The Woodcock tracking method was used to efficiently track particles in a voxel phantom. It is reasonably effective and precise for the photon energy <140 keV applied in most X-ray CT scanners.

In our previous studies, a parameterized and fully validated GE LightSpeed Pro 16 multi-detector CT (MDCT) scanner model was developed using MCNP(53, 63). We integrated this scanner model into the ARCHER code. The scanner and USTC phantoms are illustrated in Figure 4. ARCHER provides selectable scan protocols that vary in kVps, beam thicknesses, axial or helical scan modes, head or body bowtie filters. The absorbed doses to organs or tissue were normalized to a single particle. They were further mapped to the absolute dose values using our experimentally derived calibration coefficients(64).

Organ dose calculations

Absorbed doses (in the units of MeV/g/particle), which were normalized to one photon for specified organs, could be gathered from ARCHER code. A series of conversation factors (CF) demonstrated in the previous studies(53, 65) were used to convert results from ARCHER code to the absolute absorbed doses

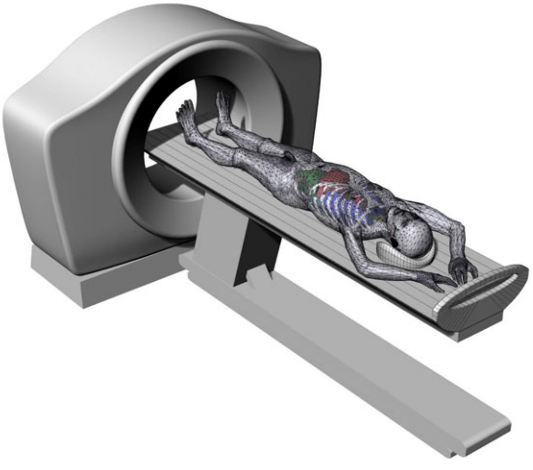

Figure 4. The newly developed USTC-AM phantom integrated with the CT scanner model and the ARCHER code for MC code simulation of various CT examination procedures.

in units of mGy/100 mAs. The conversion function is defined as follows:

$$D^{\mathrm{E,NT}}_{\mathrm{absolute}} = \left(\sum_{N} D^{\mathrm{E,NT}}_{\mathrm{simulated}} \cdot \mathrm{CF}^{\mathrm{E,NT}} \right) \cdot \mathrm{K} \tag{2}$$

where $D^{\mathrm{E,NT}}_{\mathrm{absolute}}$ is the absorbed dose in mGy; $D^{\mathrm{E,NT}}_{\mathrm{simulated}}$ in MeV/g/particle is the absorbed dose computed by our custom-built ARCHER code; $\mathrm{CF}^{\mathrm{E,NT}}$ is the conversion factor measured for GE LightSpeed Pro 16 CT scanner in the unit of (mGy/100 mAs)/(MeV/g/particle); N is the number of CT rotation slices, K is the ratio of total tube current (mAs) to 100 mAs. Equation (2) is valid under prescribed beam energy (E, kVp) and beam collimation (NT, mm). A linear interpolation algorithm[53] is adopted to calculate doses located at the beginning and the end due to the non-integral parameter N.

The stochastic radiation efforts on the whole body could be evaluated by the effective dose, E. It is computed as weighted organ equivalent doses involving gender-averaged value following by:

$$E = \sum_{\mathrm{T}} W_{\mathrm{T}} \left[\frac{H_{\mathrm{T}}^{\mathrm{M}} H_{\mathrm{T}}^{\mathrm{F}}}{2} \right] \quad (3)$$

where W_T is the weighting factor for specified tissue or organ T defined in the ICRP publication 103[66], $\mathrm{H}_{\mathrm{T}}^{\mathrm{M}}$ and $\mathrm{H}_{\mathrm{T}}^{\mathrm{F}}$ are the equivalent doses of T in the male and female phantoms, respectively.

Table 4. Scan ranges for CT scans.

Phantom	Head scan		Chest–abdomen–pelvis (CAP) scan	
	Start (cm)	End (cm)	Start (cm)	End (cm)
USTC-5M	98.0	109.9	49.6	88.2
USTC-5F	98.0	109.9	49.6	88.2
USTC-10M	125.8	138.9	65.6	113.1
USTC-10F	125.8	139.0	66.6	115.1
USTC-15M	152.2	167.5	77.8	138.0
USTC-15F	144.4	158.3	74.8	133.3
USTC-AM	156.0	169.5	78.9	139.5
USTC-AF	144.6	159.6	76.0	132.1
RPI-AM	163.5	175.6	91.9	149.5
RPI-AF	151.4	162.6	84.5	137.9

Simulations of clinical CT scan parameters

The head and chest–abdomen–pelvis (CAP) scan protocols were investigated in this study. CT scans were simulated with 120 kVp and 100 mAs, 20 mm collimation width and one pitch. Scan ranges were manually measured from voxel phantoms and summarized from AAPM CT protocols as listed in Table 4[67]. In this study, the head filter was selected in head scan protocol and the body filter was selected in CAP protocol for comparisons.

RESULTS AND DISCUSSION

Phantom results

Eight new mesh-based and age-dependent Chinese phantoms were developed: USTC-AM, USTC-AF, USTC-15M, USTC-15F, USTC-10M, USTC-10F, USTC-5M, USTC-5F. A total of 70 internal organs or tissues, 45 bone components and 4 muscle structures are contained in each single newly developed phantom. Figure 5 displays the 3D rendering of these adult phantoms and Figure 6 represents the geometries for teenager phantoms.

Representative dimensional data were stated in Tables 5–8. It is easy to calculate the trunk section height value from the body height (Table 5), the head height (Table 6) and the perinal height (Table 8);

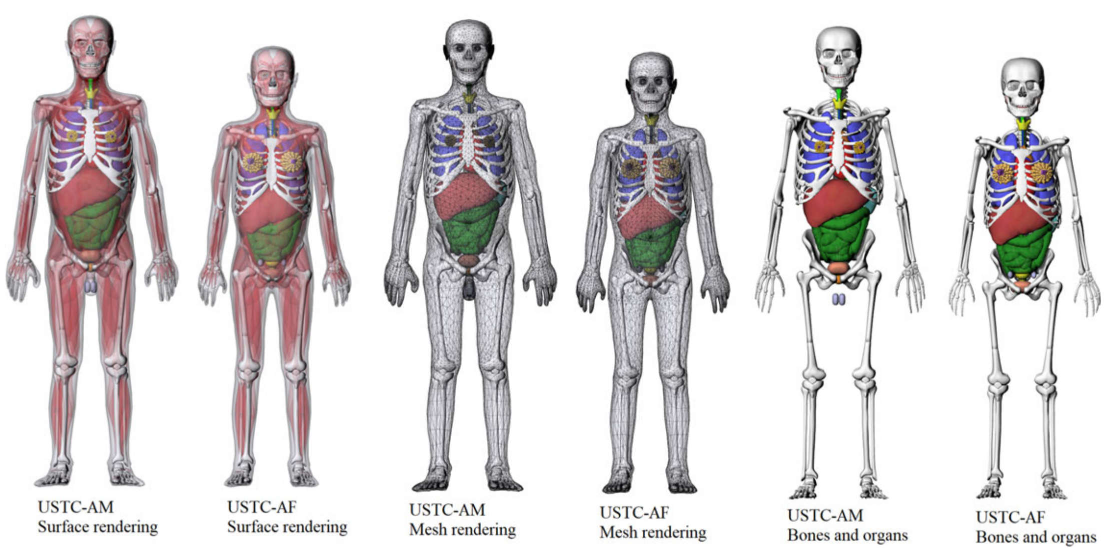

Figure 5. 3D rendering of the resulting mesh-based USTC adult male and female phantoms. Muscle tissues are only plotted in surface rendering pictures for clear exhibitions.

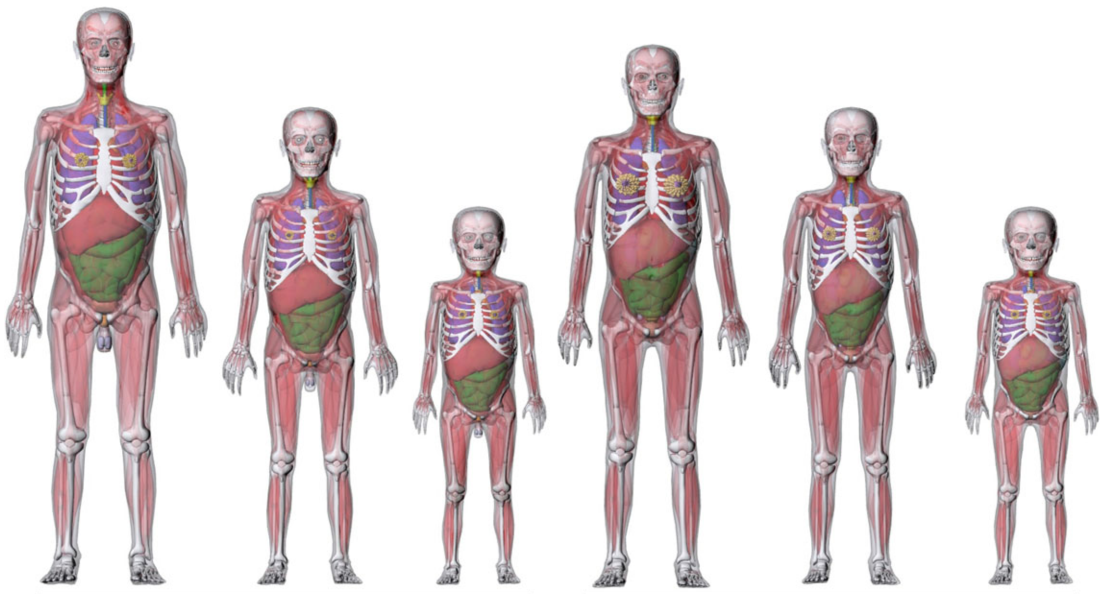

Figure 6. 3D rendering of the resulting USTC teenage mesh phantoms.

Table 5. The value of stature for USTC phantoms.

Phantom	Practical (cm)	Reference (cm)	Relative error (%)
USTC-AM	170	170	0
USTC-AF	158	158	0
USTC-15 M	168	168	0
USTC-15 F	158	158	0
USTC-10 M	139	139	0
USTC-10F	139	139	0
USTC-5M	110	110	0
USTC-5F	110	110	0

Table 6. The head height for USTC phantoms.

Phantom	Practical (cm)	Reference (cm)	Relative error (%)
USTC-AM	23.78	23.69	0.38
USTC-AF	22.95	22.82	0.57
USTC-15M	23.43	23.30	0.57
USTC-15F	22.44	22.70	1.16
USTC-10M	22.00	21.85	0.67
USTC-10F	21.40	21.65	1.18
USTC-5M	20.18	20.60	2.02
USTC-5F	20.18	20.20	0.08

therefore, the trunk height data were not listed. As exposited in these tables, the dimensions differences between USTC phantoms and reference values were small enough. They are in good accordance with the reference parameters.

CT dose results

Validation of the ARCHER code

The calculations in this study were done by ARCHER which significantly reduced the computation time. Extensive validation of ARCHER was performed using MCNPX and Geant4[62, 68]. The results from ARCHER agree with results from MCNPX very well for X-ray CT imaging doses. The percentage differences from MCNPX are <2%.

Table 7. The arm length for USTC phantoms.

Phantom	Practical (cm)	Reference (cm)	Relative error (%)
USTC-AM	75.848	73.46	0.03
USTC-AF	69.362	68.12	0.02
USTC-15M	73.589	72.25	0.02
USTC-15F	67.13	67.75	0.01
USTC-10M	59.24	59.85	0.01
USTC-10F	58.17	59.6	0.02
USTC-5M	45.91	46.7	0.02
USTC-5F	45.91	46.1	0.00

In this project, we validated the ARCHER code with MCNPX. The same GE LightSpeed Pro 16

Table 8. The perinal height for USTC phantoms.

Phantom	Practical (cm)	Reference (cm)	Relative error (%)
USTC-AM	75.15	74.17	1.33
USTC-AF	69.84	69.47	0.54
USTC-15M	73.95	72.95	1.38
USTC-15F	70.02	69.1	1.33
USTC-10M	60.42	60.6	0.30
USTC-10F	62.03	61.45	0.94
USTC-5M	45.57	44.9	1.49
USTC-5F	45.57	45.2	0.82

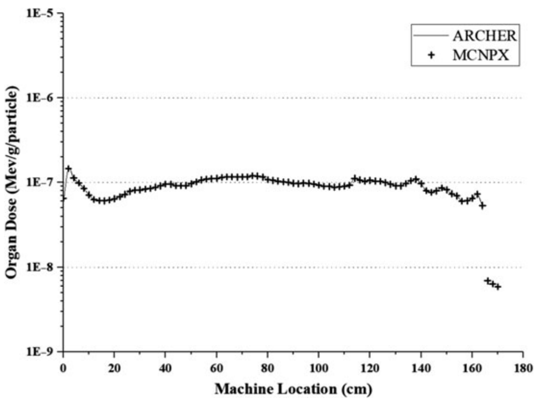

Figure 7. Dose comparisons of ARCHER with MCNPX for skin tissue.

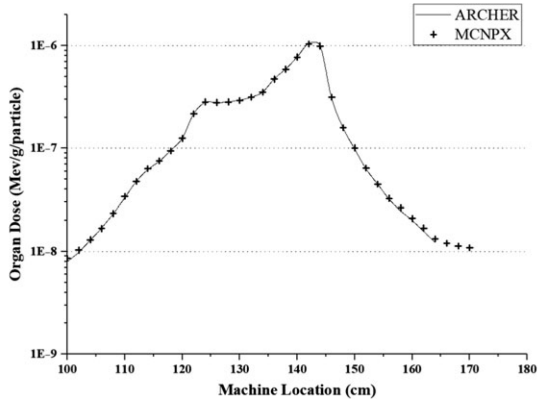

Figure 8. Dose comparisons of ARCHER with MCNPX for esophagus tissue.

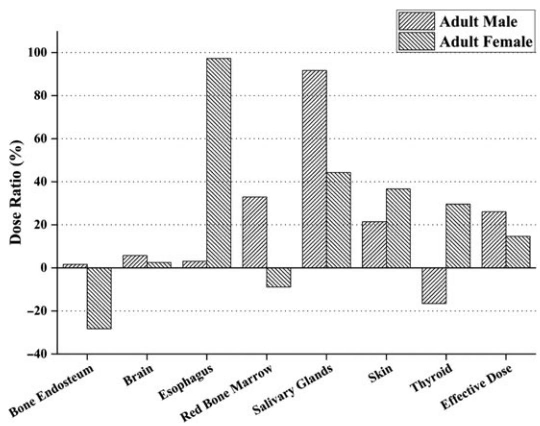

Figure 9. Dose comparisons of USTC adult phantoms with RPI adult phantoms in head scan protocol conditions. Dose values <0.5 mGy are not included. The ratio was calculated by using $(\mathrm{Dose}_{\mathrm{USTC\ Adult\ male\ or\ female}} - \mathrm{Dose}_{\mathrm{RPI\ Adult\ male\ or\ female}})/\mathrm{Dose}_{\mathrm{RPI\ Adult\ male\ or\ female}}$.

MDCT scanner model and verified adult female obese phantom model[3, 22] were combined in ARCHER and MCNPX. CT scans were simulated with 120 kVp, 20 mm collimation width and 1 pitch from the bottom of phantom to the top. To reduce relative statistical error, up to 1e7 particles were settled. Organ doses were obtained and some organ dose value differences are depicted in Figures 7 and 8. The organ doses calculated by ARCHER are in good agreement with those by MCNPX, generally within 1% when the relative uncertainty is also 1%.

Comparison of serial USTC phantom organ dose data with VirtualDose

Using the procedures described earlier, organ doses were obtained and their value differences are depicted in Figures 9 and 10. As illustrated, most of organ doses and effective doses of USTC-AM and USTC-AF phantoms are higher than RPI-AM and AF phantoms. Because of the anatomical dependency for the relative absorb dose to a particular organ or tissue these differences are expected. Generally, the dimensions of USTC adult phantoms are less than RPI adult phantoms, and the mass value for a single organ is smaller than that in the Caucasian. Because of the above points, relative absorb doses in USTC adult phantoms are higher. As for bone endosteum, absorbed doses of USTC-AF are 30% less than RPI-AF dose data. One of the reasons is that the voxel size of RPI-AF is 0.27 cm, which is too large to fully cover the thin cortical bones of skull. Some big voxels were discarded when judging whether a voxel is inside or outside the mesh according to the round-off ruler of the ray-stabbing algorithm[69, 70]. In addition, there are no orderly trends for thyroid, esophagus and salivary glands.

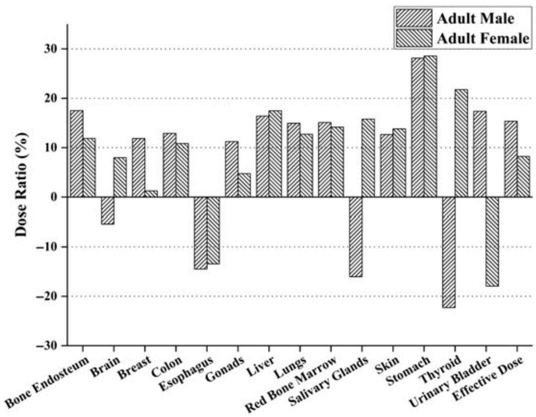

Figure 10. Dose comparisons of USTC adult phantoms with RPI adult phantoms in CAP scan protocol conditions. Dose value <0.5 are not included. The ratio was calculated by using $(\mathrm{Dose}_{\text{USTC Adult male or female}} - \mathrm{Dose}_{\text{RPI Adult male or female}})/\mathrm{Dose}_{\text{RPI Adult male or female}}$.

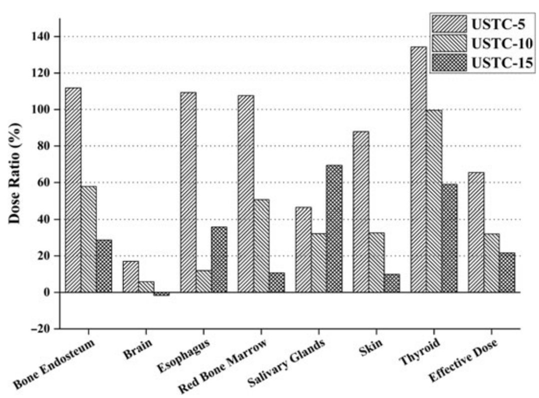

Figure 11. Plots of gender-averaged organ dose differences for phantoms in different ages in the condition of Head CT scan. Dose value <0.5 are not included. The ratio was calculated by using $(\mathrm{Dose}_{\text{USTC specified age}} - \mathrm{Dose}_{\text{USTC Adult}})/\mathrm{Dose}_{\text{USTC Adult}}$.

These three type organs are small and narrow, which make them sensitive for positions. Therefore, it is worth noting that small changes of scan ranges can make big differences.

The results in Figures 11 and 12 showed that organ doses and effective doses increased with the decrease of phantom ages. When comparing the differences between different ages, it was found that the 5-year old phantoms have the largest dose data, due to the dimensions of smaller phantoms and organs located closer to the body surfaces. For the above reasons, additional efforts should be taken to optimize CT scan protocols for teenagers, such as the utilizations of Automatic Exposure Control (AEC)

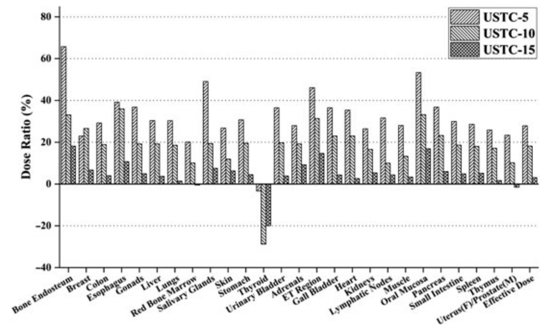

Figure 12. Plots of gender-averaged organ dose differences for phantoms in different ages in the condition of CVP CT scan. Dose value <0.5 are not included. The ratio was calculated by using $(\mathrm{Dose}_{\text{USTC specified age}} - \mathrm{Dose}_{\text{USTC Adult}})/\mathrm{Dose}_{\text{USTC Adult}}$.

technique, minimum of scanning length and reduction of repeated scanning[71, 72].

CONCLUSION

A set of mesh-based and age-dependent adult and adolescent Chinese phantoms, USTC-AM, USTC-AF, USTC-15M, USTC-15F, USTC-10M, USTC-10 F, USTC-5M, USTC-5F, have been developed by considering data from both the Chinese standards and the IAEA recommendations for the Asian population. A pair of previously developed mesh-based phantoms, RPI-AM/RPI-AF were chosen as the initial phantom. The original RPI-AM and RPI-AF phantoms, which represent adults, were scaled to create new phantoms with desired heights. At the end of the scaling step, reparative attempts were taken to fix gaps and to smooth discrete commissures. Specific fine-tuning techniques such as mesh offset, mesh scale and box edit operations were employed to change volume and shape of organs until organ-level parameters agreed within 0.5% with the reference Chinese data. All phantoms were voxelized for MC dose calculations. Voxel dimension of 0.2 cm were selected to balance compute time and anatomical reality. We used the GPU-accelerated, highly optimized ARCHER code to perform the accurate and fast simulation. The GE LightSpeed Pro 16 MDCT scanner were also modeled in ARCHER code. The newly developed phantoms were coupled with the scanner model in ARCHER, to compute doses from routine CT exams. The results indicate that organ doses for USTC phantoms, which have smaller body dimensions, are higher than those from RPI adult phantoms due to less radiation attenuation. Similarly, teenagers receive more radiation doses than adults do under the same irradiation conditions. Such dosimetric differences observed between USTC phantoms and RPI phantoms—

which differ mostly in the body dimensions—underscore the importance in considering population-specific anatomical information in radiation protection dosimetry. These phantoms and the derived organ dose information are helpful to meet the demands of nuclear power industry and medical imaging which are developing rapidly in China.

ACKNOWLEDGEMENTS

Some researchers in University of Science and Technolody of China (USTC) assisted with the revision and submission of this article: Yaping Qi, Mang Feng, Wanli Huo, Lian Zhang and Prof. Xi Pei. Data analysis were finished with the help of Ms Yaping Qi and Ms Lingli Mao. The Center of Radiological Medical Physics (CRMP) in USTC supplied the high-performance simulation server with 80 CPU cores and Nvidia K40 GPU.

FUNDING

This work was supported by research funding from the National Natural Science Foundation of China (Grant nos. 11375181 and 11375182) and the National Key Research and Development (R&D) Program of China (Grant no. 2017YFC0107504).

REFERENCES

1. Gao, Y., Quinn, B., Mahmood, U., Long, D., Erdi, Y., Germain, J. S., Pandit-Taskar, N., Xu, X. G., Bolch, W. E. and Dauer, L. T. *A comparison of pediatric and adult CT organ dose estimation methods*. BMC Med. Imaging **17**, 28 (2017).
2. OECD. *Health Care Use—Computed Tomography (CT) Exams-OECD Data* (2017). Available on http://data.oecd.org/healthcare/computed-tomography-ct-exams.htm.
3. Liang, B., Gao, Y., Chen, Z. and Xu, X. G. *Evaluation of effective dose from CT scans for overweight and obese adult patients using the VirtualDose software*. Radiat. Prot. Dosim. **174**(2), 216–225 (2016).
4. Mettler, F. A., Jr, Bhargavan, M., Faulkner, K., Gilley, D. B., Gray, J. E., Ibbott, G. S., Lipoti, J. A., Mahesh, M., McCrohan, J. L. and Stabin, M. G. *Radiologic and nuclear medicine studies in the United States and worldwide: frequency, radiation dose, and comparison with other radiation sources—1950–07*. Radiology **253**(2), 520–531 (2009).
5. Mettler, F. A., Jr, Thomadsen, B. R., Bhargavan, M., Gilley, D. B., Gray, J. E., Lipoti, J. A., McCrohan, J., Yoshizumi, T. T. and Mahesh, M. *Medical radiation exposure in the US in 2006: preliminary results*. Health Phys. **95**(5), 502–507 (2008).
6. Turner, A. C., Zankl, M., DeMarco, J. J., Cagnon, C. H., Zhang, D., Angel, E., Cody, D. D., Stevens, D. M., McCollough, C. H. and McNitt-Gray, M. F. *The feasibility of a scanner-independent technique to estimate organ dose from MDCT scans: using CTDIvol to account for differences between scanners*. Med. Phys. **37** (4), 1816–1825 (2010).
7. Xu, X. G. *An exponential growth of computational phantom research in radiation protection, imaging, and radiotherapy: a review of the fifty-year history*. Phys. Med. Biol. **59**(18), R233–R302 (2014).
8. Xu, X. G. and Eckerman, K. F. *Handbook of Anatomical Models for Radiation Dosimetry* (Boca Raton: CRC Press) (2009).
9. Snyder, W. S., Ford, M. R., Warner, G. G. and Fisher, H. L., Jr *Estimates of absorbed fractions for monoenergetic photon sources uniformly distributed in various organs of a heterogeneous phantom*. J. Nucl. Med. **Suppl 3**, 7–52 (1969).
10. Eckerman, K. F., Poston, J., Bolch, W. and Xu, X. G. *The stylized computational phantoms developed at ORNL and elsewhere*. In: Handbook of Anatomical Models for Radiation Dosimetry. **Vol. 14**, Xu, X.G. and Eckerman, K.F. Eds (Boca Raton: Taylor & Francis) pp. 43–64 (2009).
11. Lim, S.-M., DeNardo, G. L., DeNardo, D. A., Shen, S., Yuan, A., ODonnell, R. and DeNardo, S. *Prediction of myelotoxicity using radiation doses to marrow from body, blood, and marrow sources*. J. Nucl. Med. **38**, 1374 (1997).
12. Zaidi, H. and Xu, X. G. *Computational anthropomorphic models of the human anatomy: the path to realistic Monte Carlo modeling in radiological sciences*. Ann. Rev. Biomed. Eng. **9**, 471–500 (2007).
13. International Commission On Radiological Protection ICRP Publication 89. *Basic anatomical and physiological data for use in radiological protection: reference values*. Ann. ICRP **32**(3), 1–277 (2002).
14. Zhang, J., Na, Y. H., Caracappa, P. F. and Xu, X. G. *RPI-AM and RPI-AF, a pair of mesh-based, size-adjustable adult male and female computational phantoms using ICRP-89 parameters and their calculations for organ doses from monoenergetic photon beams*. Phys. Med. Biol. **54**, 5885 (2009).
15. International Commission On Radiological Protection ICRP Publication 23. *Report on the task group on reference man*. Ann. ICRP **48**(2), 285–285 (1985).
16. United Nations Scientific Committee on the Effects of Atomic. *Sources, effects and risks of ionizing radiation*. UNSCEAR 2013 Report: Volume II: Scientific Annex B: Effects of radiation exposure of children (2013).
17. Brenner, D., Elliston, C., Hall, E. and Berdon, W. *Estimated risks of radiation-induced fatal cancer from pediatric CT*. AJR Am. J. Roentgenol. **176**(2), 289–296 (2001).
18. Brenner, D. J. *Estimating cancer risks from pediatric CT: going from the qualitative to the quantitative*. Pediatr. Radiol. **32**(4), 228-1 (2002) ; discussion 242. 4.
19. Shah, N. B. and Platt, S. L. *ALARA: is there a cause for alarm? Reducing radiation risks from computed tomography scanning in children*. Curr. Opin. Pediatr. **20**(3), 243–247 (2008).
20. Council, N. R. *Health Risks From Exposure to Low Levels of Ionizing Radiation: BEIR VII Phase 2* (Washington, DC: National Academies Press) (2006).
21. Na, Y. H., Zhang, B., Zhang, J., Caracappa, P. F. and Xu, X. G. *Deformable adult human phantoms for radiation protection dosimetry: anthropometric data representing size distributions of adult worker populations and software algorithms*. Phys. Med. Biol. **55**, 3789 (2010).

22. Ding, A., Mille, M. M., Liu, T., Caracappa, P. F. and Xu, X. G. *Extension of RPI-adult male and female computational phantoms to obese patients and a Monte Carlo study of the effect on CT imaging dose*. Phys. Med. Biol. **57**(9), 2441–2459 (2012).
23. Hegenbart, L., Na, Y. H., Zhang, J. Y., Urban, M. and Xu, X. G. *A Monte Carlo study of lung counting efficiency for female workers of different breast sizes using deformable phantoms*. Phys. Med. Biol. **53**(19), 5527–5538 (2008).
24. Cassola, V. F., Milian, F. M., Kramer, R., de Oliveira Lira, C. and Khoury, H. J. *Standing adult human phantoms based on 10th, 50th and 90th mass and height percentiles of male and female Caucasian populations*. Phys. Med. Biol. **56**, 3749 (2011).
25. de Melo Lima, V. J., Cassola, V. F., Kramer, R., de Oliveira Lira, C. A. B., Khoury, H. J. and Vieira, J. W. *Development of 5-and 10-year-old pediatric phantoms based on polygon mesh surfaces*. Med. Phys. **38**(8), 4723–4736 (2011).
26. Christ, A. *et al*. *The Virtual Family—development of surface-based anatomical models of two adults and two children for dosimetric simulations*. Phys. Med. Biol. **55** (2), N23 (2009).
27. Lee, C., Lodwick, D., Hurtado, J., Pafundi, D., Williams, J. L. and Bolch, W. E. *The UF family of reference hybrid phantoms for computational radiation dosimetry*. Phys. Med. Biol. **55**(2), 339 (2010).
28. Geyer, A. M., O'Reilly, S., Lee, C., Long, D. J. and Bolch, W. E. *The UF/NCI family of hybrid computational phantoms representing the current US population of male and female children, adolescents, and adults-application to CT dosimetry*. Phys. Med. Biol. **59**(18), 5225–5242 (2014).
29. GBZ. *Reference Individuals for Use in Radiation Protection Part 1: Physique Parameters* (Beijing: People's Medical Publishing House) (2007).
30. Kawamura, H., Tanaka, G.-i., Shiraishi, K., Honda, Y., Nishimuta, M., Koyanagi, T., Karim, F., Molla, M., Rab, A. and Wang, J. *Compilation of anatomical, physiological and metabolic characteristics for a Reference Asian Man-IAEA-TECDOC-1005*. J. Radiat. Res. (Tokyo) **39**(4), 350 (1998).
31. Tanaka, G., Kawamura, H., Griffith, R. V., Cristy, M. and Eckerman, K. F. *Reference man models for males and females of six age groups of Asian populations*. Radiat. Prot. Dosim. **79**(1–4), 383–386 (1998).
32. Wang, J., Chen, R., Zhu, H., Zhou, Y. and Ma, R. *Data of Anatomical Physiological and Metabolic Characteristics for Chinese Reference Man* (Beijing, Atomic Energy Press) (1999).
33. Zhang, B., Ma, J., Liu, L. and Cheng, J. *CNMAN: a Chinese adult male voxel phantom constructed from color photographs of a visible anatomical data set*. Radiat. Prot. Dosim. **124**(2), 130–136 (2007).
34. Zhang, G., Liu, Q., Zeng, S. and Luo, Q. *Organ dose calculations by Monte Carlo modeling of the updated VCH adult male phantom against idealized external proton exposure*. Phys. Med. Biol. **53**, 3697 (2008).
35. Li, J., Qiu, R., Zhang, Z., Liu, L., Zeng, Z., Bi, L. and Li, W. *Organ dose conversion coefficients for external photon irradiation using the Chinese voxel phantom (CVP)*. Radiat. Prot. Dosim. **135**, 33–42 (2009).
36. Liu, L., Zeng, Z., Li, J., Qiu, R., Zhang, B., Ma, J., Li, R., Li, W. and Bi, L. *Organ dose conversion coefficients on an ICRP-based Chinese adult male voxel model from idealized external photons exposures*. Phys. Med. Biol. **54**(21), 6645 (2009).
37. Zhang, B., Ma, J., Zhang, G., Liu, Q., Qiu, R. and Li, J. *Chinese voxel computational phantoms: CNMAN, VCH, and CVP*. In: Handbook of Anatomical Models for Radiation Dosimetry. **Vol. 279**, Xu, X.G. and Eckerman, K.F. Eds (Boca Raton: Taylor & Francis) pp. 279–303 (2009).
38. Pan, Y., Qiu, R., Gao, L., Ge, C., Zheng, J., Xie, W. and Li, J. *Development of 1-year-old computational phantom and calculation of organ doses during CT scans using Monte Carlo simulation*. Phys. Med. Biol. **59**, 5243–5260 (2014).
39. Kawrakow, I. and Rogers, D. The EGSnrc code system: Monte Carlo simulation of electron and photon transport (2000).
40. Battistoni, G., Cerutti, F., Fasso, A., Ferrari, A., Muraro, S., Ranft, J., Roesler, S. and Sala, P. *The FLUKA Code: Description and Benchmarking* (Melville, NY: AIP) pp. 31–49 (2007).
41. Agostinelli, S., Allison, J., Amako, K., Apostolakis, J., Araujo, H., Arce, P., Asai, M., Axen, D., Banerjee, S. and Barrand, G. *GEANT4-a simulation toolkit*. Nucl. Instrum. Methods A **506**(3), 250–303 (2003).
42. Pelowitz, D. B. *MCNPX User's Manual Version 2.5.0*. Los Alamos National Laboratory. 76 (2005).
43. Salvat, F., Fernández-Varea, J. M. and Sempau, J. *PENELOPE-2008: A Code System for Monte Carlo Simulation of Electron and Photon Transport*. In: The Workshop Proceedings (2008).
44. Robert, C. P. *Monte Carlo Methods* (Hoboken, NJ: Wiley Online Library) (2004).
45. Andreo, P. *Monte Carlo techniques in medical radiation physics*. Phys. Med. Biol. **36**(7), 861–920 (1991).
46. Liu, T., Xu, X. G. and Carothers, C. D. *Comparison of two accelerators for Monte Carlo radiation transport calculations, Nvidia Tesla M2090 GPU and Intel Xeon Phi 5110p coprocessor: a case study for X-ray CT imaging dose calculation*. Ann. Nucl. Energy **82**, 230–239 (2015).
47. Liu, T. *Development of ARCHER—a Parallel Monte Carlo Radiation Transport Code—for X-ray CT Dose Calculations Using GPU and Coprocessor Technologies*. (Ann Arbor: Rensselaer Polytechnic Institute (RPI)) (2012).
48. Xu, X. G., Taranenko, V., Zhang, J. and Shi, C. *A boundary-representation method for designing whole-body radiation dosimetry models: pregnant females at the ends of three gestational periods—RPI-P3,-P6 and-P9*. Phys. Med. Biol. **52**, 7023 (2007).
49. ImPACT. *impactscan.org|ctdosimetry.xls—ImPACT's CT Dosimetry Tool* (2011). Available on http://www.impactscan.org/ctdosimetry.htm.
50. Stamm, G. and Nagel, H. D. *CT-expo—a novel program for dose evaluation in CT*. Rofo **174**, 1570–1576 (2002).
51. Cros, M., Joemai, R., Geleijns, J., Molina, D. and Salvadó, M. *SimDoseCT: dose reporting software based on Monte Carlo simulation for a 320 detector-row cone-beam CT scanner and ICRP computational adult phantoms*. Phys. Med. Biol. **62**(15), 6304–6321 (2017).
52. VirtualPhantoms Inc. *VirtualDose—SaaS Radiation Exposure Dose Software |VirtualDose* (2013). Available on http://www.virtual-dose.com.

53. Ding, A., Gao, Y., Liu, H., Caracappa, P. F., Long, D. J., Bolch, W. E., Liu, B. and Xu, X. G. *VirtualDose: a software for reporting organ doses from CT for adult and pediatric patients*. Phys. Med. Biol. **60**(14), 5601 (2015).
54. International Commission On Radiological Protection ICRP Publication 70. *Basic anatomical & physiological data for use in radiological protection—the skeleton*. Ann. ICRP **25**(2), 1–80 (1995).
55. GBZ. *Reference Individuals for Use in Radiation Protection Part 2: Masses of Main Organs and Tissues* (Beijing, People's Medical Publishing House) (2007).
56. GBZ. *Reference Individuals for Use in Radiation Protection Part 5: Human Body Elemental Composition and Contents of Element in Main Tissues and Organs* (Beijing, People's Medical Publishing House) (2009).
57. International Commission On Radiological Protection ICRP Publication 110. *Realistic reference phantoms: an ICRP/ICRU joint effort. A report of adult reference computational phantoms*. Ann. ICRP **39**(2), 1 (2009).
58. Zankl, M., Eckerman, K. and Bolch, W. *Voxel-based models representing the male and female ICRP reference adult—the skeleton*. Radiat. Prot. Dosim. **127**, 174–186 (2007).
59. Cassola, V., Kramer, R., de Melo Lima, V., de Oliveira Lira, C., Khoury, H., Vieira, J. and Brown, K. R. *Development of newborn and 1-year-old reference phantoms based on polygon mesh surfaces*. J. Radiol. Prot. **33**, 669 (2013).
60. Robert McNeel & Associates. *Rhinoceros* (2014). Available on https://www.rhino3d.com/.
61. International Commission on Radiation Units & Measurements. *ICRU Report 46: Photon, electron, proton and neutron interaction data for body tissues*. ICRU Report. 46 (1992).
62. Xu, X. G. *et al*. *ARCHER, a new Monte Carlo software tool for emerging heterogeneous computing environments*. Ann. Nucl. Energy **82**, 2–9 (2015).
63. Ding, A., Gu, J., Trofimov, A. V. and Xu, X. G. *Monte Carlo calculation of imaging doses from diagnostic multidetector CT and kilovoltage cone-beam CT as part of prostate cancer treatment plans*. Med. Phys. **37**(12), 6199–6204 (2010).
64. Ding, A. *Development of a Radiation Dose Reporting Software for X-ray Computed Tomography (CT)* ((Ann Arbor, Rensselaer Polytechnic Institute (RPI))) (2012).
65. Gu, J., Bednarz, B., Caracappa, P. F. and Xu, X. G. *The development, validation and application of a multidetector CT (MDCT) scanner model for assessing organ doses to the pregnant patient and the fetus using Monte Carlo simulations*. Phys. Med. Biol. **54**(9), 2699–2717 (2009).
66. International Commission On Radiological Protection ICRP Publication 103. *The 2007 Recommendations of the International Commission on Radiological Protection*. Ann. ICRP **37**(2–4), 1–332 (2007).
67. American Association of Physicists in Medicine. *AAPM CT Scan Protocols—The Alliance for Quality Computed Tomography* (2017). Available on http://www.aapm.org/pubs/CTProtocols/.
68. Su, L., Yang, Y., Bednarz, B., Sterpin, E., Du, X., Liu, T., Ji, W. and Xu, X. G. *ARCHER-RT, A photon-electron coupled Monte Carlo dose computing engine for GPU: software development and application to helical tomotherapy*. Med. Phys. **41**(7), 071709 (2014).
69. Lane, J. and Carpenter, L. *A generalized scan line algorithm for the computer display of parametrically defined surfaces*. Comput. Graph. Image Process. **11**(3), 290–297 (1979).
70. Nooruddin, F. S. and Turk, G. *Simplification and repair of polygonal models using volumetric techniques*. IEEE Trans. Vis. Comput. Graph. **9**(2), 191–205 (2003).
71. International Commission On Radiological Protection. *ICRP Publication 102. Managing Patient Dose in Multi-detector Computed Tomography (MDCT)* (Elmsford, NY: Elsevier) (2007).
72. Vock, P., Stranzinger, E. and Wolf, R. *Dose Optimization and Reduction in CT of Children* (Berlin, Heidelberg: Springer) (2012).